The dynamics of three coupled dipolar Bose–Einstein condensates*

Wu Jian-Hua(武建华)[a)†] and Xu Sheng-Nan(许胜男)[b)]

[a)] *Beijing National Laboratory for Condensed Matter Physics, Institute of Physics, Chinese Academy of Sciences, Beijing* 100190, *China*

[b)] *Center for Computer Information, Hebei Normal University for Nationalities, Chengde* 067000, *China*

(Received 15 April 2013; revised manuscript received 9 May 2013)

The dynamics of the three coupled dipolar Bose–Einstein condensates containing N bosons is investigated within a mean-field semiclassical picture based on the coherent-state method. Varieties of periodic solutions (configured as vortex, single depleted well, and dimerlike states) are obtained analytically when the fixed points are identified on the $N =$ constant. The system dynamics are studied via numeric integration of trimer motion equations, thus revealing macroscopic effects of population inversion and self-trapping with different initial states. In particular, the trajectory of the oscillations of the populations in each well shows how the dynamics of the condensates are effected by the presence of dipole–dipole interaction and gauge field.

Keywords: Bose–Einstein condensate, triple-well, dipole–dipole interaction, dynamics

PACS: 03.75.Kk, 03.75.Lm, 03.65.Sq **DOI:** 10.1088/1674-1056/22/12/120304

1. Introduction

Great progress in experimental design has been made since the first achievement of Bose–Einstein condensation (BEC) of dilute gases in 1995.[1,2] It has formed one of the main topics of research at the moment and marked the beginning of a new era in optical physics, condensed matter physics, quantum optics, and so on. Nowadays, ultra-cold atomic and molecular systems are at the frontier of modern quantum physics, and are seriously considered to offer more control than solid-state systems.[3–5] We know that quantum gases are very dilute systems, in the ultra-cold regime only s-wave scattering between particles can take place. This makes us replace the real interatomic potential by a pseudo-potential, which is short range, isotropic and characterized by the s-wave scattering length a. For a large number of atomic species, the magnitude and even the sign of the scattering length a can be tuned by means of an external magnetic field. This phenomenon, called Feshbach resonance,[6,7] has found multiple applications since its first experimental observation in cold gases.[8,9]

The interaction pseudo-potential, despite its simplicity, plays a crucial role in the static and dynamic properties of Bose–Einstein condensates;[10,11] one of the most fascinating properties they are responsible for is the superfluid character of those gases. There has been a great quantity of previous investigations analyzing the dynamics[12] and the quantum tunneling of Bose–Einstein condensates. Smerzi *et al.* deliberated the occurrence of macroscopic self-trapping within one well in Ref. [13]. In Refs. [14]–[16] the behavior of the system during an adiabatic change of parameters was researched and the Landau–Zener formula and generalizations of the linear two-level crossing scenarios were analyzed. Ran *et al.* investigated the non-Abelian Josephson effect between two $F = 2$ spinor Bose–Einstein condensates in double optical traps in Ref. [17]. Liu *et al.* investigated the Wannier–Stark intraband transitions in lattice potentials under gravity in Ref. [18] and in Ref. [19] the Josephson effect for photons in two weakly linked microcavities has been considered by Ji *et al.* Another line of investigation considers the mesoscopic regime in which semiclassical techniques can be used to study the system.[20–25]

But recently, dipolar quantum gases, in which the anisotropic and long-range dipole–dipole interaction (DDI) between dipole moments plays a remarkable, even dominant role, have drawn much attention for they show engaging novel properties. For those reasons, there has been a quest for realizing quantum gases with different, richer interactions in order to study these interesting properties. BECs in optical lattices with DDI have become a fascinating field of experimental and theoretical interest and much attention has been paid to explore the effects of the DDI by employing different models.[26,27] Tie *et al.* investigated the anisotropy of dipole–dipole interaction of a dipolar condensate in one-dimensional optical lattices. They found that the tunneling rate between Bloch bands, the Bloch band structure, and the stabilities of it can be controlled by adjusting the effective aspect ratio of the condensate and the dipolar orientation.[28] In Ref. [29], the matter-wave interference was studied in an axial triple-well optical dipole trap and the local field distribution functions of up-spins

*Project supported by the National Key Basic Research Special Foundation of China (Grant Nos. 2011CB921502, 2012CB821305, 2009CB930701, and 2010CB922904), the National Natural Science Foundation of China (Grant Nos. 10934010, 11228409, and 61227902), and the National Natural Science Foundation of China–The Research Grants Council (Grant Nos. 11061160490 and 1386-N-HKU748/10).

†Corresponding author. E-mail: wjh@iphy.ac.cn

© 2013 Chinese Physical Society and IOP Publishing Ltd

for systems of dipolar interaction with particular emphasis on Ising-type lattice systems was investigated systematically in Ref. [30].

In this paper we present a semiclassical method to analyze the spectral properties of a dipolar BEC in a triple-well potential, which presents clear visual nonlocal features of DDI. This technique has been used to investigate the vibrational spectra of molecules[31–34] and provides a presentative picture for the inexplainable spectra at first glance. In the circumstances, the dynamics of a dipolar BEC in a triple well potential is parallel to the vibrations of a triatomic molecule. We introduce a simple semiclassical method of visualization and classification of the quantum eigenstates to describe the dipolar quantum system by using the geometrical language. We perform a systematic analysis of the trimer dynamics to ascertain that the absence of integrability dominates the interactions of the three dipolar BECs modeled in a standard semiclassical picture, and the analysis provides a thorough scenario of the trimer dynamical regimes and of their dependence on the external parameters occurring in the Hamiltonian which is expected to be operationally useful in relative experiments.

This paper is organized as follows. In Section 2, we retrospect the derivation of the Hamiltonian for three coupled BECs from the quantum field theory of bosonic fluids in the dilute-gas approximation, and advance the semiclassical picture that describes three coupled wells with macroscopic populations. In Section 3, we confirm the set of fixed points of the trimer Hamiltonian equations. Section 4 is devoted to perform a dimensional reduction of trimer dynamics by defining a new set of canonical variables whereby the constant of motion N is incorporated in the dynamical equations. Section 5 contains conclusions and some comments on future work.

2. The model and trimer dynamics

As shown in Fig. 1, we consider a system consisting of boson gases in an external potential $V_{\rm trap}$. If the boson fluid is a dilute gas of N interacting bosons, that is to say, a weak two-particle pointlike interaction can be assumed, then the Hamiltonian in the second quantization can be written as

$$\widehat{H} = \int \mathrm{d}\boldsymbol{r}\,\widehat{\psi}^{\dagger}(\boldsymbol{r},t)\left[V_{\rm trap}(\boldsymbol{r},t) - \frac{\hbar^2\nabla^2}{2m} + \frac{g}{2}\widehat{\psi}^{\dagger}(\boldsymbol{r},t)\widehat{\psi}(\boldsymbol{r},t) + V_{\rm dd}(\boldsymbol{r},t)\right]\widehat{\psi}(\boldsymbol{r},t), \tag{1}$$

where m is the mass of the particles, $g = 4\pi a_s\hbar^2/m$ is the coupling constant of the two-body interaction strength, and a_s is the s-wave scattering length. For an attractive interaction g is negative, while for a repulsive interaction g takes a positive value.

$$V_{\rm dd}(\boldsymbol{r}) = \int \left|\widehat{\psi}(\boldsymbol{r}')\right|^2 U_{\rm dd}(\boldsymbol{r}-\boldsymbol{r}')\,\mathrm{d}\boldsymbol{r}'$$

takes into account the dipole–dipole interaction strength, and

$$U_{\rm dd}(r) = \frac{C_{\rm dd}}{4\pi}\frac{1-3\cos^2\theta}{r^3}.$$

The operator $\widehat{\psi}^{\dagger}(\boldsymbol{r})$ $[\widehat{\psi}(\boldsymbol{r})]$ is the Heisenberg field operator that creates (annihilate) bosons at position r which can be expanded as $\widehat{\psi}(\boldsymbol{r}) = \sum_{i=1}^{3}\phi_i(\boldsymbol{r})\widehat{a}_i(t)$, where $\widehat{a}_i(t)$ $[\widehat{a}_i^{\dagger}(t)]$ is the annihilation (creation) boson operator that satisfies the commutation relation $[\widehat{a}_i(t),\widehat{a}_j^{\dagger}(t)] = \delta_{i,j}$. Then by substituting this expression in the second quantization Hamiltonian, we get the quantum trimer Hamiltonian

$$H(a_i,a_i^{\dagger}) = -J\sum_{i,j}[a_i^{\dagger}a_j + \text{H.c.}] + \frac{U_0}{2}\sum_{i}^{3}n_i(n_i-1) + U_1\sum_{i}^{3}n_in_{i+1}, \tag{2}$$

where

$$J = -\int \mathrm{d}\boldsymbol{r}\,\phi_1(\boldsymbol{r})\left[-\hbar^2\frac{\nabla^2}{2m} + V_{\rm trap}(\boldsymbol{r})\right]\phi_2(\boldsymbol{r})$$

is the hopping rate,

$$U_0 = g\int |\phi_1(\boldsymbol{r})|^4\,\mathrm{d}\boldsymbol{r} + \int |\phi_1(\boldsymbol{r})|^2|\phi_1(\boldsymbol{r}')|^2U_{\rm dd}(\boldsymbol{r}-\boldsymbol{r}')\,\mathrm{d}\boldsymbol{r}\,\mathrm{d}\boldsymbol{r}'$$

characterizes the on-site interactions, and

$$U_1 = \int |\phi_1(\boldsymbol{r})|^2|\phi_2(\boldsymbol{r}')|^2 \times U_{\rm dd}(\boldsymbol{r}-\boldsymbol{r}')\,\mathrm{d}\boldsymbol{r}\,\mathrm{d}\boldsymbol{r}'$$

is the coupling constant for nearest-neighbor DDI (dipole–dipole interaction). The site index $i,j = 1,2,3$, and the operators $n_i = a_i^{\dagger}a_i$ counts the bosons at site i.

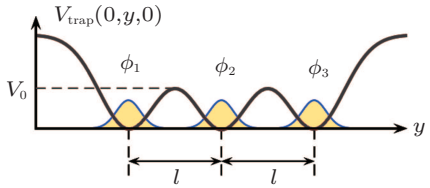


Fig. 1. (color online) The experimental schematic diagram of the three-well system. The wells are aligned at the y axis, separated by an energy barrier V_0 and a distance l. The atoms were polarized by a strong external field with a dipole moment $\boldsymbol{d}$ along a fixed direction. We assume that compared to other energies (especially the interaction energies), the lattice potential is strong enough so that the on-site wave functions $\phi_{i=1,2,3}(\boldsymbol{r})$ are fixed, which is independent of the number of bosons per well.

By representing the system quantum state through a trial state $|Z\rangle = \prod_i|z_i\rangle$ written in terms of Glauber's states $|z_i\rangle$ (defined by $a_i|z_i\rangle = z_i|z_i\rangle$), the quantum dynamics involved by Hamiltonian $H(a_i,a_i^{\dagger})$ can be cast in a classical form. The effective Hamiltonian can be obtained by implementing the time-dependent variational principle (TVDP), we get

$$H(z,z^*) = \langle Z|H|Z\rangle = \sum_{i=1}^{3}[-J(z_i^*z_{i+1} + c.c) + \frac{U_0}{2}(|z_i|^4 - |z_i|^2)$$

$$+U_1|z_i|^2|z_{i+1}|^2], \tag{3}$$

($i=1\equiv 4$ on the trimer chain) with the equations for the triple-well dynamics

$$\begin{aligned}
\mathrm{i}\hbar\dot{z}_1 &= -J(z_2+z_3)+\frac{U_0}{2}(|z_1|^2-1)z_1+U_1(|z_2|^2+|z_3|^2)z_1,\\
\mathrm{i}\hbar\dot{z}_2 &= -J(z_3+z_1)+\frac{U_0}{2}(|z_2|^2-1)z_2+U_1(|z_1|^2+|z_3|^2)z_2,\\
\mathrm{i}\hbar\dot{z}_3 &= -J(z_1+z_2)+\frac{U_0}{2}(|z_3|^2-1)z_3+U_1(|z_1|^2+|z_2|^2)z_3,
\end{aligned} \tag{4}$$

here we implement the randomphase approximation in the equations for their expectation values $z_i=\langle Z|a_i|Z\rangle$, $z_i^*=\langle Z|a_i^\dagger|Z\rangle$, and the dynamics equations for z_i can be calculated from $H(z,z^*)$ by the Poisson brackets $\{z_i^*,z_j\}=(\mathrm{i}/\hbar)\delta_{i,j}$.

3. Fixed points of the Hamiltonian

The distinguishing features characterizing a given Hamiltonian dynamic are deduced by exploring the structure of its phase space. The first step to do this[35,36] is to find out the location of the fixed points of the Hamiltonian and to find their dependence on the model parameters J, U_0, and U_1. Since the constant of motion $N=\sum_{i=1}^3|z_i|^2$ constrains the trimer dynamics, one must involve the restriction to the phase-space submanifold definitely defined by $N=$ const through a Lagrange multiplier χ. This requires us to consider the variations of $H-\chi N$ in place of that of H. For Eqs. (4), the fixed points can be obtained by setting $\dot{z}_i=0$. Then we get the equations

$$\begin{aligned}
0 &= -J(z_2+z_3)+\left(\frac{U_0}{2}|z_1|^2-\mu\right)z_1+U_1\left(|z_2|^2+|z_3|^2\right)z_1,\\
0 &= -J(z_3+z_1)+\left(\frac{U_0}{2}|z_2|^2-\mu\right)z_2+U_1\left(|z_1|^2+|z_3|^2\right)z_2,\\
0 &= -J(z_1+z_2)+\left(\frac{U_0}{2}|z_3|^2-\mu\right)z_3+U_1\left(|z_1|^2+|z_2|^2\right)z_3,
\end{aligned} \tag{5}$$

where $\mu=U_0/2+\chi$, the set of Eqs. (5) is equal to

$$-JZ+\left[\left(\frac{U_0}{2}-U_1\right)|z_i|^2+J+U_1N-\mu\right]z_i=0, \tag{6}$$

where $i=1,2,3$, and $Z=z_1+z_2+z_3$. Hence, any vector $(z_i)\equiv(\tau_1,\tau_2,\tau_3)$ that satisfies Eqs. (6) provides a dynamically active solution of Eqs. (4) represented by $z_i(t)=\tau_i\exp[\mathrm{i}\chi t/\hbar]$. Such a periodic orbit represents an extremal configuration of H on the hypersurface $N=$ const despite its time dependence. The solutions of Eqs. (6) can be grouped in different classes, the first of which is represented by the case

$$Z=\sum_j z_j=0. \tag{7}$$

Noting the invariance of Eqs. (6) under the global symmetry transformation $z_l\to z_l\exp(\mathrm{i}\Phi)$ and the fact that $z_l/Z\in R$ with $l=1,2,3$, we can set $z_l=x_l\exp(\mathrm{i}\Phi)$, where the x_l are real numbers and Φ is an arbitrary phase, thus equations (6) reduce to a system of the three-real equations

$$E_j(x):=\left[\left(\frac{U_0}{2}-U_1\right)x_j^2+J-\mu+U_1N\right]x_j-JX\equiv 0, \tag{8}$$

with $X=x_1+x_2+x_3$, and $j=1,2,3$. When we impose the condition $x_i\neq 0$ for $i=1,2,3$, the sum of the quantities $E_j(x)/x_j$ can be set to be equal to zero provided $x_j\neq 0$ thus giving the equation

$$3\mu=\left(\frac{U_0}{2}+2U_1\right)N-J\sum_i\frac{X-x_i}{x_i}. \tag{9}$$

Besides, form $E_1(x)/x_1-E_2(x)/x_2=0$ and $E_2(x)/x_2-E_3(x)/x_3=0$ we obtain

$$(x_2-x_1)\left[\left(\frac{U_0}{2}-U_1\right)(x_2+x_1)+\frac{JX}{x_1x_2}\right]=0, \tag{10}$$

$$(x_2-x_3)\left[\left(\frac{U_0}{2}-U_1\right)(x_2+x_3)+\frac{JX}{x_2x_3}\right]=0, \tag{11}$$

completed by the condition $N=x_1^2+x_2^2+x_3^2$.

Thus we obtain the remaining cases from Eqs. (10) and (11), where z_i can be replaced by the real quantities x_i. Such cases are given by $x_1=x_2=x_3\neq 0$, $x_1=-x_3\neq x_2=0$, and $x_1=x_2\neq x_3\neq 0$ which will be discussed below.

3.1. Ground-state configuration

When $x_1=x_2=x_3$, based on Eq. (3) combined with the conserved quantity N, we find that $x_j=\pm\sqrt{N/3}$ which provides

$$z_i=\sqrt{N/3}\exp(\mathrm{i}\Phi),\quad (i=1,2,3), \tag{12}$$

and $(U_0/2+2U_1)N-6J-3\mu=0$. Then we can give the energy of such configurations

$$E_{\mathrm{gs}}=\frac{1}{3}\left(\frac{U_0}{2}+2U_1\right)N^2-JN. \tag{13}$$

Since the ground-state phase represents the symmetry of the model, it is arbitrary. Also, the fact that $z_j=|z_j|\exp(\mathrm{i}\phi_j)$ has the same phase which reproduces the symmetry breaking phenomenon that distinguishes the vanishing of the phase difference between closed points and the minimum energy state in superfluid media. Such two features are known to characterize the superfluid ground state of the Bose–Hubbard lattice model, and to extend to the trimer model of condensates in our semiclassical picture naturally.

3.2. Vortexlike configurations

The $Z=0$ situation leads to a special configuration. In the circumstances equations (6) reduce to

$$\left[\left(\frac{U_0}{2}-U_1\right)|z_i|^2+J+U_1N-\mu\right]z_i=0$$

implying that

$$|z_i|^2=2\frac{\mu-J-U_1N}{U_0-2U_1},\ \ \forall j,$$
$$\mu=\frac{1}{3}\left(\frac{U_0}{2}+2U_1\right)N+J, \tag{14}$$

where from $\sum_i|z_i|^2=N$ we can derive the value of μ. With the result that the independence of $|z_i|$ on the site index, the condition $Z=0$ can be realized only if the phases of $z_i=|z_i|\exp(\mathrm{i}\theta_i)$ are satisfied with that $\theta_i(k)=2\pi\mathrm{i}k/3+\Phi_0$, where $k=1,2$, and Φ_0 is an arbitrary phase. The vortex states energy is given by

$$\begin{aligned}E_v&=\frac{(U_0+2U_1)N^2}{12}-2JN\cos\left(\frac{2\pi}{3}k\right)\\&=\frac{(U_0+2U_1)N^2}{12}+JN,\end{aligned} \tag{15}$$

with

$$z_i(k)=\sqrt{N/3}\exp(\mathrm{i}\theta_i(k)), \tag{16}$$

while the dynamics of Eqs. (4) are described by the solution $z_i(t)=z_i(k)\exp[\mathrm{i}t(\mu-U_0)/\hbar]$.

3.3. Configurations with a single depleted well

These configurations are characterized by the existence of a single depleted well (SDW). Without losing generality, we choose the second well, so that we have $x_1,x_3\neq 0$, and $x_2=0$. This can be faced based on Eqs. (8): we must impose $x_1=-x_3$ to satisfy $E_2(x)=0$, with the addition of constraint $N=x_1^2+x_3^2$, implies that $x_1=\pm\sqrt{N/2}=-x_3,x_2=0$, then we get the fixed points

$$z_1=\sqrt{N/2}\,\mathrm{e}^{\mathrm{i}\Phi},\ \ z_2=0,\ \ z_3=\sqrt{N/2}\,\mathrm{e}^{\mathrm{i}(\Phi+\pi)}, \tag{17}$$

with $\mu\equiv(U_0/2+2U_1)N+J$. The energy of this configuration is

$$E_{\mathrm{SDW}}=\frac{(U_0+4U_1)N^2}{4}+JN. \tag{18}$$

The permutations of site index i of z_i furnish another five fixed points of the same type. In consideration of state (17), it is worth noting that configurations with an SDW have the same structure of the π states occurring in the dimer dynamics, where the phase of each well keeps a constant phase difference π in process of time evolution. Solutions

$$z_i(t)=z_i(0)\exp\left[\mathrm{i}t\left(\mu-\frac{U_0}{2}+U_1\right)/\hbar\right]$$

of SDW with $z_i(0)$ given by Eqs. (17) exhibit the same property.

3.4. Dimerlike configurations

For such states, the variables x_i satisfy the condition $x_i=x_j\neq x_k$. Through index permutation, three cases are thus obtained. In general, nine fixed points are finally found in the dimerlike class since three fixed points turn out to be associated with each dimerlike configuration.

To deal with a definite case, we consider the following case $x_1=x_2\neq x_3$. Because of the identification $x_1=x_2$, equations (10) and (11) become a unique equation that can be written as

$$\left(\frac{U_0}{2}-U_1\right)(x_1^2-x_3^2)=J\left(1+\frac{x_3}{x_1}-2\frac{x_1}{x_3}\right). \tag{19}$$

Such an expression allows us to parametrize x_1 and x_3 in two possible ways,

$$\begin{aligned}x_1&=\sqrt{N}R\cosh\alpha,\ \ x_3=\sqrt{N}R\sinh\alpha;\\x_1&=\sqrt{N}R\sinh\beta,\ \ x_3=\sqrt{N}R\cosh\beta,\end{aligned} \tag{20}$$

both of these parametrizations allowing for the elimination of N in the constraint $2x_1^2+x_3^2\equiv N$. In the first case, we find

$$R^2=\frac{1-q^2}{2+q^2},\ \ R^2=\frac{\tau}{4}\left(1+q-\frac{2}{q}\right), \tag{21}$$

whereas the second case gives

$$R^2=\frac{1-p^2}{1+2p^2},\ \ R^2=\frac{\tau}{4}\left(2p-1-\frac{1}{p}\right), \tag{22}$$

where $\tau=4J/(U_0-2U_1)N$, $q=\tanh\alpha$, $p=\tanh\beta$, and $\alpha,\beta\in R$. System (21) reduces to the cubic equation

$$\tau(q^2+2)(q+2)+4q(q+1)=0, \tag{23}$$

which, provided $q\in[-1,1]$ in order to ensure the condition $R^2\geq 0$, supplies either none or two solutions, depending on the fact that $\tau>\tau^*,\tau<\tau^*$. Then we find that by solving the system, the two roots $q_\nu(\tau),\nu=1,2$ fulfil the conditions

$$-1\leq q_1(\tau)\leq q_2(\tau)\leq 0\ \ \text{for}\ \ 0\leq\tau\leq\tau^*, \tag{24}$$

with $q_1(\tau)=q_2(\tau)$ for $\tau=\tau^*$. By imposing the requirement that the two q-dependent functions of Eqs. (21) be tangent at some point,

$$\frac{-6q}{(2+q^2)^2}\equiv\frac{\tau}{2}\left(1+\frac{2}{q^2}\right), \tag{25}$$

the parameter τ^* is identified, in addition to Eq. (23), and we obtain the value $\tau^*\simeq 0.2972$ by solving numerically.

Such a formation does not characterize system (22), which always reveals a single solution for some appropriate value obtained from the equation in the sector $p\in[-1/2,0]$

$$\tau(p^2+2)(p+2)+2p(p+1)=0. \tag{26}$$

In consideration of the restriction $q, p < 0$, from the definition (20) we conclude that $x_1 x_3 < 0$. The three solutions $q_1(\tau)$, $q_2(\tau)$, $p(\tau)$ just obtained correspond to three vectors, within the space of coordinates $\{(x_1, x_2, x_3)\} \equiv \boldsymbol{R}^3$, expressed as

$$\begin{aligned} A_1 &= (a_1, a_1, -(a_1/|a_1|)\sqrt{N-2a_1^2}), \\ A_2 &= (a_2, a_2, -(a_2/|a_2|)\sqrt{N-2a_2^2}), \\ A_3 &= (a_3, a_3, -(a_3/|a_3|)\sqrt{N-2a_3^2}), \end{aligned} \tag{27}$$

where

$$a_\nu = \pm\left[\frac{N}{2+q_\nu^2}\right]^{1/2}, \nu = 1,2, a_3 = \pm\left[\frac{Np^2}{1+2p^2}\right]^{1/2}, \tag{28}$$

which can be derived from $q = \tanh\alpha$, $\cosh^2(\alpha) - \sinh^2(\alpha) = 1$ and $p = \tanh\beta$, $\cosh^2(\beta) - \sinh^2(\beta) = 1$, with q_υ and p defined as implicant functions of parameter τ through Eqs. (21) and (22), respectively. The dependence on parameters J, U_0, U_1, N of $A_1(q_1)$, $A_2(q_2)$, $A_3(p)$ by means of τ are thus established.

Points A_i found in this way generate three curves with $N =$ const by varying τ. These become 9 when considering the fixed points generated by index permutations,

$$\begin{aligned} B_1 &= \left(a_1, -(a_1/|a_1|)\sqrt{N-2a_1^2}, a_1\right), \\ C_1 &= \left(-(a_1/|a_1|)\sqrt{N-2a_1^2}, a_1, a_1\right), \\ B_2 &= \left(a_2, -(a_2/|a_2|)\sqrt{N-2a_2^2}, a_2\right), \\ C_2 &= \left(-(a_2/|a_2|)\sqrt{N-2a_2^2}, a_2, a_2\right), \\ B_3 &= \left(a_3, -(a_3/|a_3|)\sqrt{N-2a_3^2}, a_3\right), \\ C_3 &= \left(-(a_3/|a_3|)\sqrt{N-2a_3^2}, a_3, a_3\right), \end{aligned} \tag{29}$$

related to the subcases $x_1 = x_3 \neq x_2$ and $x_2 = x_3 \neq x_1$. Due to the double choice $\pm$ in Eqs. (28) such curves are 18.

If the values of q_υ and p are carried out for some certain $\tau \leq \tau^*$ explicitly, the energy for A_i is obtained by formulas (28),

$$\begin{aligned} E_D &= \left(\frac{U_0}{2} + 2U_1\right)[N^2 + 6a_i^4 - 4Na_i^2] \\ &\quad - J\left[a_i^2 - 2a_i\sqrt{N-2a_i^2}\right], \quad (i = 1,2,3). \end{aligned} \tag{30}$$

When τ changes, we conclude to illustrate the physical situations which correspond to configurations A_1, A_2, A_3. Let us begin with $\tau \to 0$. We have $q_1 = -1$ and $q_2 = p = 0$ that entail $A_1(-1) := \pm(\sqrt{N/3}, \sqrt{N/3}, -\sqrt{N/3})$, $A_2(0) := (\sqrt{N/2}, \sqrt{N/2}, 0)$, $A_3(0) := (0, 0, \sqrt{N})$, respectively. When τ is increasing, $A_1(q_1)$ and $A_2(q_2)$ get closer and closer. When $\tau > \tau^*$ only the fixed point $A_3(p)$ exists. Among others, $\tau \to \infty$ implies $p = -1/2$, so that we obtain $A_3(-1/2) = \pm(\sqrt{N/6}, \sqrt{N/6}, -\sqrt{2N/3})$.

At last, we want to see that state $A_1(-1)$ exhibits the same per-well boson distribution as the ground state. Such two states differ one and only to the phase of the third well. In a similar manner, the π-like state $(\sqrt{N/2}, -\sqrt{N/2}, 0)$ and state $A_1(0)$ just differ owing to the opposite phase of the second well. The finding by our analysis is that the stability character for dimerlike states exhibits two saddle points and one maximum point for $0 < \tau < \tau^*$.

4. The dynamics on the reduced phase space

Hamiltonian (3) commutes with the boson number N and depends on three complex degrees of freedom. This fact is the same as the structure of the coupling term in $H(Z, Z^*)$ which allows us to reduce the number of canonical coordinates from six to four. This can be achieved by replacing the complex coordinates $z_i = \sqrt{n_i}\exp(\mathrm{i}\theta_i)$ with

$$\begin{aligned} \phi_1 &= \theta_2 - \theta_1, \ \xi_1 = (n_2 + n_3 - n_1)/N, \\ \phi_2 &= \theta_3 - \theta_2, \ \xi_2 = (n_3 - n_2 - n_1)/N, \\ \psi &= (\theta_1 + \theta_3)/2, \ N = n_1 + n_2 + n_3, \end{aligned} \tag{31}$$

which obey the canonical Poisson brackets $\{\phi_i, N\} = 0$, $\{\xi_i, \phi_j\} = 2\delta_{ij}/N$, $\{\xi_i, \psi\} = 0$, $\{\psi, N\} = -1$. With such new variables the effective Hamiltonian (3) becomes

$$\begin{aligned} &H(\xi_1, \xi_2, \phi_1, \phi_2) \\ &= \varepsilon_0 + (\frac{U_0}{4} - \frac{U_1}{2})N^2(\xi_2 - \xi_1 - \xi_1\xi_2 + \xi_1^2 + \xi_2^2) \\ &\quad - JN[\sqrt{(1-\xi_1)(\xi_1 - \xi_2)}(\cos A\cos\phi_1 - \sin A\sin\phi_1) \\ &\quad + \sqrt{(\xi_1 - \xi_2)(1+\xi_2)}(\cos A\cos\phi_2 - \sin A\sin\phi_2) \\ &\quad + \sqrt{(1-\xi_1)(1+\xi_2)}(\cos A\cos\phi_{12} + \sin A\sin\phi_{12})], \end{aligned} \tag{32}$$

where $\varepsilon_0 = (U_0/4 - U_1/2)N^2 - \mu N$ and A is an arbitrary phase caused by gauge field. Then in terms of coordinates $(\xi_1, \xi_2, \phi_1, \phi_2)$ the ground-state fixed points and vortexlike configuration correspond to

$$\left(\frac{1}{3}, -\frac{1}{3}, 0, 0\right), \ \left(\frac{1}{3}, -\frac{1}{3}, \frac{2}{3}\pi k, \frac{2}{3}\pi k\right), \ (k = 1,2), \tag{33}$$

respectively. SDW states can be expressed as $(0, 0, \varphi, \pi - \varphi)$ for $n_2 = 0$ and dimerlike fixed points (consider A_1 in Eqs. (27)) are given by $(\xi_1, 2\xi_1 - 1, \pi, -\pi)$ where $\xi_1 = 1 - 2a_1^2(\tau)/N$ and $a_1(\tau)$ is defined by Eqs. (28).

5. Discussion of numerical results

We now present the results of the numerical analysis and investigate the phenomenology of the trimer dynamics within the initial conditions close to the fixed points.

5.1. Ground state initial conditions

Figure 2 shows the typical time evolution of the condensates' populations related to a motion with initial conditions close to a ground-state configuration. We can see that, when $A = 0$, $U_0 = J \simeq 2U_1$, the condensates' populations of each well keep intact as time goes on. When we increase U_1 to $U_1 \simeq 3U_0/2$, the oscillations of the condensates' populations occur after a certain time, the reason for this is that the dipole–dipole interaction is a long range interaction which can lead to a quantum tunneling when it is strong enough. But when $A \neq 0$, the populations of each well will keep constant no matter how strong the dipole–dipole interaction. This is a very interesting phenomenon which indicates that the gauge field enhances the stability of the ground state.

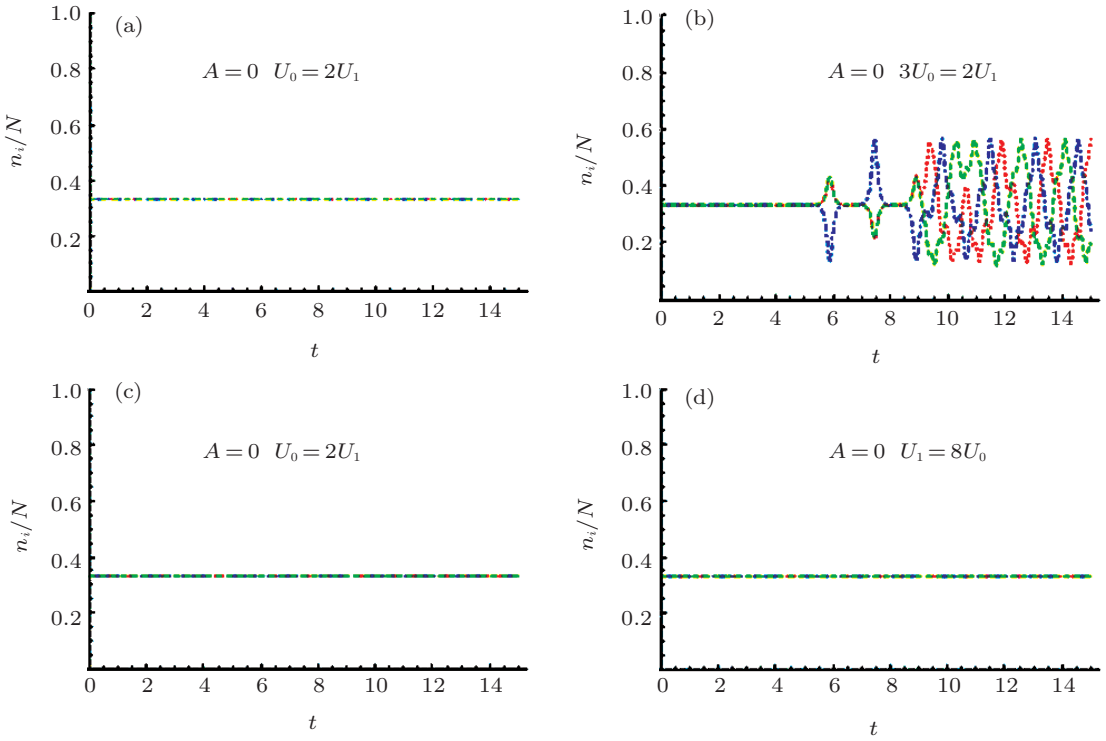


Fig. 2. (color online) (a) Typical time evolution of the condensates' populations related to a motion with initial conditions close to a ground-state configuration without gauge field. The red dotted, blue dot-dashed, green dashed lines refer to $n_1(t)$, $n_2(t)$, and $n_3(t)$ respectively. (b) Time evolution of condensate populations $n_1(t)$ (red doted line), $n_2(t)$ (blue dot-dashed line), and $n_3(t)$ (green dashed line) when U_1 increased to $U_1 = 1.5U_0$. (c) and (d) Populations n_1 (red doted line), n_2 (blue dot-dashed line), and n_3 (green dashed line) are plotted as a function of the time in the presence of gauge field.

5.2. Vortexlike initial conditions

The initial conditions for the dynamics have been chosen close to the fixed points $(\xi_1, \phi_1) = (1/3, 2k\pi/3)$, $k = 1, 2$, (vortex state). Since no difference distinguishes the trajectories with $k = 1$ and that with $k = 2$, we pay attention to $k = 1$. First of all, let us consider the situation of $A = 0$. Figure 3 shows the time evolution of n_i when $U_0 = J \simeq 2U_1$, we can see that the population of each well oscillated regularly and respectively with the same frequency. Then we increase U_1 to $U_1 \simeq 3U_0/2$, the frequency of oscillations will go up and the trajectories will become irregular in one oscillating period but regular for a long time (see Fig. 4). If we continue to increase U_1, the oscillations will become faster and faster, in other words, the stronger the dipole–dipole interaction is, the faster the oscillations are. When $A \neq 0$, the effect of the gauge field will make the oscillations become more complicated. But these effects can be classfied into two types, one type is that the gauge field makes the oscillations of the condensates more regular, the other type is that the gauge field makes the amplitude of the oscillations bigger and bigger as time goes on. $A = \pi/3$ and $A = \pi/2$ are two typical representatives of the oscillations (see Fig. 5).

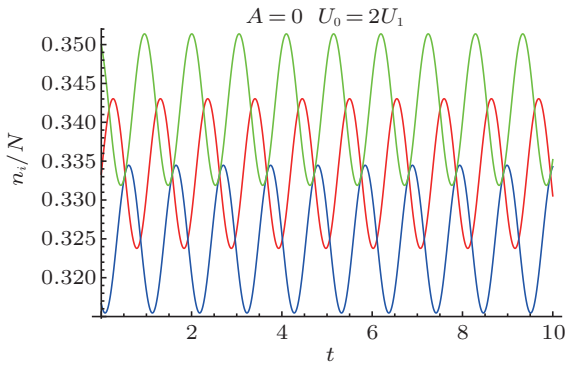


Fig. 3. (color online) The figure plots the populations $n_1(t)$ (red line), $n_2(t)$ (blue line), and $n_3(t)$ (green line) as a function of the time, for the initial conditions chosen close to vortexlike state with $U_0 = 2U_1$.

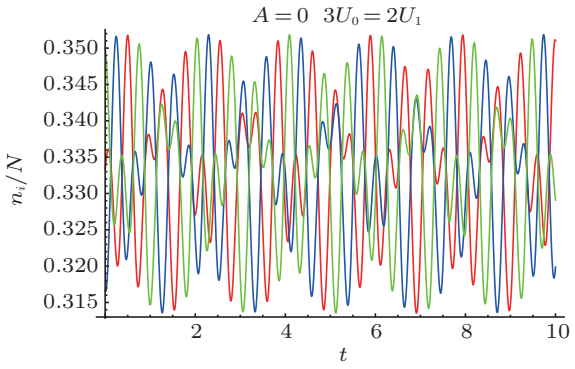


Fig. 4. (color online) Populations of three condensates: $n_1(t)$ (red line), $n_2(t)$ (blue line), and $n_3(t)$ (green line) as a function of time for the initial conditions chosen close to vortexlike fixed point with $U_1=(3/2)U_0$.

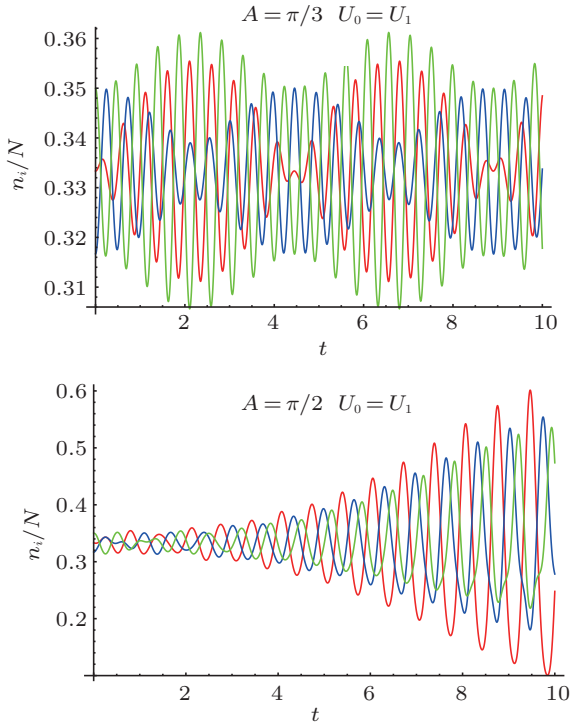


Fig. 5. (color online) Condensates' populations, as a function of the time, related to the vortexlike initial state with $U_0=U_1$ and gauge field being on the scene. The red, blue, and green lines are refer to $n_1(t)$, $n_2(t)$, and $n_3(t)$, respectively.

5.3. SDW-like intial conditions

In this case the initial conditions for the dynamics have been chosen close to $\xi_1=\xi_2=0$, $\phi_1=\varphi$, $\phi_2=\pi-\varphi$, where we have set $\xi_1=0.01$, $\xi_2=-0.01$, $\varphi=0.5\pi$ (φ can be chosen arbitrarily). Figure 6 describes the oscillations of the populations under the condition of $A=0$ and $U_0=J\simeq 2U_1$, one can see that the quantum tunneling only happens between two of the three wells, that is to say the population of the second well n_2 always keeps to zero and the presence of the gap between n_2 and n_1, n_3 indicates a macroscopic self-trapping effect. But this self-trapping differs from the self-trapping reviewed in the previous section, where $z_1=z_3\to n_1=n_3$, in that n_1, n_3 develop independent oscillations. Then we increase U_1 to $U_1=3U_0/4$ and keep $A=0$, the nonperiodic oscillations of populations $n_1(t)$, $n_2(t)$, and $n_3(t)$ are compared as shown in Fig. 7. The results indicate that the long range dipole–dipole interaction makes the quantum tunneling of the condensates more widespread. If we continue to increase U_1, the oscillations will become more and more fierce and irregular, at last, even a population-inversion effect involving $n_1(t)$, $n_2(t)$ gets going.

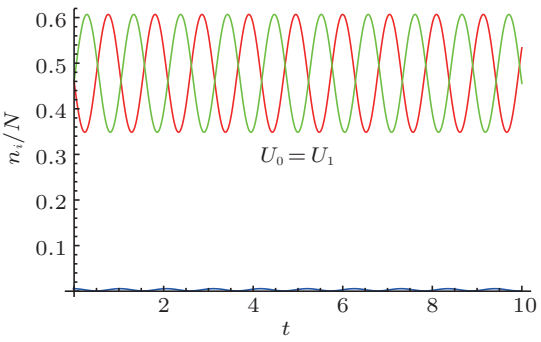


Fig. 6. (color online) Temporal behavior of the condensates' populations related to the initial conditions close to the configurations with a single depleted well (SDW). The red, green lines trace $n_1(t)$, $n_3(t)$, respectively, $n_2(t)=0$.

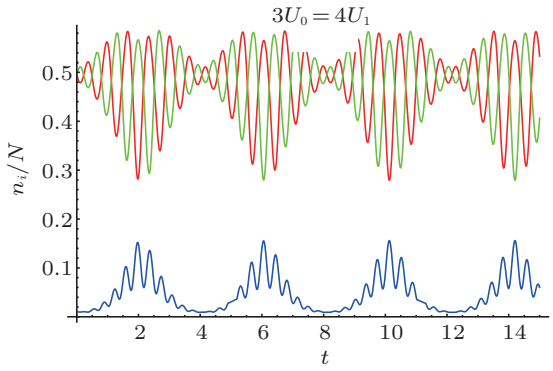


Fig. 7. (color online) Typical time evolution of the condensates' populations related to a motion with initial conditions close to a configuration with a single depleted well (SDW). The red, blue, and green lines refer to $n_1(t)$, $n_2(t)$, and $n_3(t)$, respectively.

5.4. Dimerlike initial conditions

As mentioned before, the fixed points of this case consist of two saddle points and a maximum. The conditions $\xi_1=0.295$ and $\xi_1=0.005$ firm the trajectory associated with the first saddle point with coordinates $\xi_1=-\xi_2=0.295$, $\phi_1=-\phi_2=\pi$, and to the second saddle point with $\xi_1=-\xi_2=0.005$, $\phi_1=-\phi_2=\pi$, respectively. The trajectories near the maximum $\xi_1=0.995$, $\xi_2=-0.995$, $\phi_1=-\phi_2=\pi$, appear to be the same, regularly with that of near the saddle points. So in the case of the dimerlike initial conditions, we just consider one of the three cases: maximum fixed point. In this case, populations $n_1(t)$, $n_2(t)$, and $n_3(t)$ display as shown in Fig. 8, a periodic effect of population–synchronization involving $n_1(t)$

and $n_3(t)$, whereas the fact that $n_1, n_3 \ll n_2$ entails an evident self-trapping phenomenon. Then we increased U_1 to $U_1 = U_0$, we found that the dipole–dipole interaction increased the frequency of the oscillations and enhanced the self-trapping at the same time (see Fig. 9). This is the greatest difference of the effect of the dipole–dipole interaction when compared with other initial states. These results were got at the absence of gauge field. When $A \neq 0$, the situation will become more irregular and complicated. Here we just show the simplest case for $A = \pi/3$, figure 10 describes the oscillations of the populations

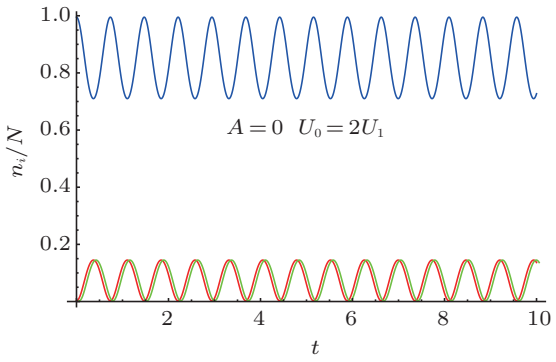


Fig. 8. (color online) Populations of three condensates: $n_1(t)$ (red line), $n_2(t)$ (blue line), and $n_3(t)$ (green line) as a function of the time for the initial conditions chosen close to a dimerlike fixed point with $U_0 = 2U_1$.

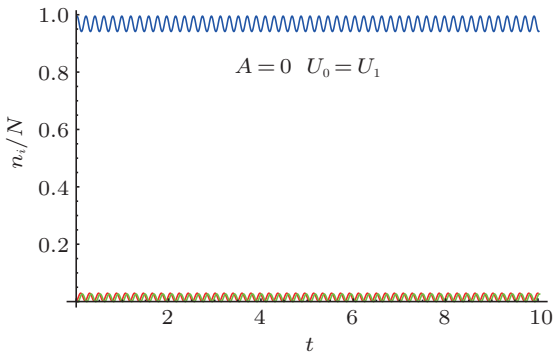


Fig. 9. (color online) The figure plots the populations $n_1(t)$ (red line), $n_2(t)$ (blue line), and $n_3(t)$ (green line) as a function of the time, for the initial conditions chosen close to a dimerlike state with $U_0 = U_1$.

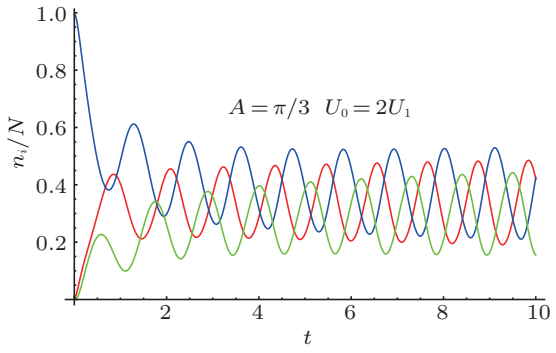


Fig. 10. (color online) Typical time evolution of the condensates' populations related to a motion with initial conditions close to a dimerlike fixed point. The red, blue, green lines refer to $n_1(t)$, $n_2(t)$, and $n_3(t)$, respectively.

for this case. We can see that the gauge field destroyed both the self-trapping and the dimerlike initial state at the very beginning and made a hypodispersion of the populations for each well with the same oscillation frequency.

6. Conclusions

In this paper, we have focused our attention on the dynamics of the phase space for the mean field form of the model describing three dipole–dipole interacting BECs. We first calculated the fixed points of the Hamiltonian to explore the structure of its phase space. Then we investigated the dynamics of the Hamiltonian in reduced phase space by reducing the number of canonical coordinates of the Hamiltonian from six to four. And at last we analyzed the numerical results, we found that the dipole–dipole interaction will increase the frequency of the oscillations of the populations and the gauge field will change the amplitude of the oscillations with different initial states. In combining with the recent experimental results, the phenomenology of this system seems more and more viable to experimental observations. In conclusion, we showed that the semiclassical method provides an intuitive picture of the quantum mechanical many-particle Hamiltonian, and allows a direct classification of the dynamics.

References

[1] Anderson M H, Ensher J R, Matthews M R, Wieman C E and Cornellet E A 1995 *Science* **269** 198
[2] Bradley C C, Sackett C A, Tollett J J and Hulet R G 1995 *Phys. Rev. Lett.* **75** 1687
[3] Giorgini S, Pitaevskii L P and Stringari S 2008 *Rev. Mod. Phys.* **80** 1215
[4] Bloch I, Dalibard J and Zwerger W 2008 *Rev. Mod. Phys.* **80** 885
[5] Lewenstein M, Sanpera A, Ahufinger V, Damski B, Sen(De) A and Sen U 2007 *Adv. Phys.* **56** 243
[6] Köhler T, Góral K and Julienne P S 2006 *Rev. Mod. Phys.* **78** 1311
[7] Chin C, Grimm R, Julienne P and Tiesinga E 2009 *Rev. Mod. Phys.* arXiv: **0812** 1496
[8] Inouye S, Andrews M R, Stenger J, Miesner H J, Stamper-Kurn D M and Ketterle W 1998 *Nature* **392** 151
[9] Courteille P, Freeland R S, Heinzen D J, van Abeelen F A and Verhaar B J 1998 *Phys. Rev. Lett.* **81** 69
[10] Pitaevskii L P and Stringari S 2003 *Bose–Einstein Condensation* (Oxford: Clarendon)
[11] Pethick C J and Smith H 2002 *Bose–Einstein Condensation in Dilute Gases* (Cambridge: Cambridge University Press)
[12] Mossmann S and Jung C 2006 *Phys. Rev. A* **74** 033601
[13] Smerzi A, Fantoni S, Giovanazzi S and Shenoy S R 1997 *Phys. Rev. Lett.* **79** 4950
[14] Witthaut D, Graefe E M and Korsch H J 2006 *Phys. Rev. A* **73** 063609
[15] Liu J, Wu B and Niu Q 2003 *Phys. Rev. Lett.* **90** 170404
[16] Wu B and Niu Q 2003 *New J. Phys.* **5** 104
[17] Qi R,Yu X L, Li Z B and Liu W M 2009 *Phys. Rev. Lett.* **102** 185301
[18] Liu W M, Fan W B, Zheng W M, Liang J Q and Chui S T 2002 *Phys. Rev. Lett.* **88** 170408
[19] Ji A C, Sun Q, Xie X C and Liu W M 2009 *Phys. Rev. Lett.* **102** 023602
[20] Milburn G J, Corney J, Wright E M and Walls D F 1997 *Phys. Rev. A* **55** 4318
[21] Smerzi A and Raghavan S 2000 *Phys. Rev. A* **61** 063601
[22] Anglin J R and Vardi A 2001 *Phys. Rev. A* **64** 013605
[23] Anglin J R, Drummond P and Smerzi A 2001 *Phys. Rev. A* **64** 063605

[24] Thommen Q, Garreau J C and Zehnlé V 2003 *Phys. Rev. Lett.* **91** 210405
[25] Mahmud K W, Perry H and Reinhardt W P 2005 *Phys. Rev. A* **71** 023615
[26] Xiong B 2009 *Phys. Rev. A* **79** 013626
[27] Asaduz Z M and Blume D 2009 *Phys. Rev. A* **80** 053622
[28] Tie L and Xue J K 2012 *Chin. Phys. Lett.* **29** 020301
[29] Zhou Q, Lu J F and Yin J P 2010 *Chin. Phys. B* **19** 093202
[30] Yan Y and Wu B 2012 *Chin. Phys. Lett.* **29** 013203
[31] Sibert E L and McCoy A B 1996 *J. Chem. Phys.* **105** 469
[32] Jacobson M P, Jung C, Taylor H S and Field R W 1999 *J. Chem. Phys.* **111** 600
[33] Jung C, Taylor H S and Atilgan E 2002 *J. Phys. Chem. A* **106** 3092
[34] Jung C, Mejia-Monasterio C and Taylor H S 2004 *J. Chem. Phys.* **120** 4194
[35] Ott E 1993 *Chaos in Dynamical Systems* (Cambridge: Cambridge University Press)
[36] Wu B, Diener R B and Niu Q 2002 *Phys. Rev. A* **66** 023404